Journal of Catalysis **192,** 344–354 (2000)
doi:10.1006/jcat.2000.2850, available online at http://www.idealibrary.com on IDEAL®

Influence of Si/Zr Ratio on the Formation of Surface Acidity in Silica–Zirconia Aerogels

James A. Anderson,*,[1] Craig Fergusson,* Inmaculada Rodríguez-Ramos,† and Antonio Guerrero-Ruiz‡

*Department of Chemistry, The University, Dundee, DD1 4HN, Scotland, U.K.; †Instituto de Catálisis y Petroleoquímica (CSIC), Campus UAM, Cantoblanco, Madrid 28049, Spain; and ‡Departamento de Química Inorgánica, UNED, Madrid 28040, Spain

Received October 15, 1999; revised January 14, 2000; accepted February 2, 2000

A series of silica–zirconia mixed oxides were prepared by sol–gel routes where the zirconia content was varied from 9 to 75 mol%. The bulk and surface properties were analysed and compared with those of a sample where zirconia was deposited as an external layer on a silica surface thereby avoiding internal mixing of the component oxides. Spin–lattice relaxation measurements made by ^{29}Si MAS NMR provide a useful estimation of the relative size of domains containing silica only and thus the degree of mixing. High levels of silica distribution throughout the mixed oxide prevented crystallisation of zirconia phases even at high Zr : Si ratios. The extent of mixing at the surface and throughout the bulk is discussed in relation to the generation of both Lewis and Brønsted acid sites. Increased levels of mixing and heteroatom linkages throughout the bulk did not necessarily result in an increase in the density of surface Brønsted acid sites generated. © 2000 Academic Press

Key Words: solid acids; silica–zirconia; acidity in mixed oxides; ^{29}Si NMR.

INTRODUCTION

Solid acids are one of the most important types of catalyst used by the oil and chemicals industries and applications will increase with moves to replace liquid acids currently used for many organic reactions. Unlike other types of catalysts, the nature of the active site is known and may be defined by the presence of surface protons, generating Brønsted acidity, or coordinately unsaturated cationic centres, i.e., Lewis acid sites (1). Mixed oxides often show greatly enhanced acid activity compared with the individual component oxides. The most widely accepted model for the generation of acid sites on mixed oxides (2) is that the surface acidity results from a charge imbalance imposed upon the minor component oxide by the imposition of the bond matrix of the major. This is an extension of an earlier charge imbalance hypothesis (3), where the minor component oxide metal retains its coordination. While this model has been claimed to be 90% correct in predictions of mixed oxide acidity (4), it fails to explain cases where 50–50 mol% mixed oxides exhibit the greatest acidity (5, 6). More recent modifications to this model (7, 8) still rely on charge imbalance resulting from heteroatom linkages for the creation of acid centres. A model based on electrostatic potential differences of a cationic centre in the two different matrices (9) again fails to incorporate the 50–50 example and furthermore the necessity for homogeneity is incompatible with the acidity shown by supported oxides. Such generalized macromodels would appear to be rather cumbersome, and it may be necessary to look to finer structural detail to explain acidity induction in these materials.

Sol–gel chemistry allows a high degree of flexibility in the formation of mixed oxides as their properties can be deliberately influenced by manipulation of their preparation parameters. Homogeneity can be controlled by alkoxide ligand type, solution temperature of the reaction process, and precursor concentration (10) whereas hydrolysis level and acid/base catalysis may strongly influence surface hydroxylation, as well as structural aspects. Aging in solution, drying conditions, and postformative thermal treatments provide additional controls (11). Aerogels are distinguished by their low density, high porosity, and high surface area. Traditional mixed oxide preparation techniques such as calcination of mechanically ground mixtures of oxides or oxide precursors, while producing well-mixed oxides, give typically very dense products, with low surface area and porosity, and are less attractive for use as industrial catalysts (1, 12). Sol–gel-derived silica–zirconia mixed oxides with a range of Si/Zr ratios have been prepared here with the objective to determine the influence of this ratio on surface acidity. This forms part of a wider study, involving sol–gel-derived samples with fixed Si/Zr ratios and samples prepared by impregnation and precipitation procedures (13, 14) where the aim was to relate the distribution of the components to the generation of surface acidity and to extend a general model to more rationally justify enhanced acidity in mixed metal oxide systems.

EXPERIMENTAL

Sample Preparation

A series of samples were prepared in which the zirconia content was varied from 9 to 75 mol%. Tetraethylortho-

[1] To whom correspondence should be addressed.

0021-9517/00 $35.00

silicate (TEOS) was combined with water, propanol, and 70 wt% nitric acid and stirred during 10 min prehydrolysis time. A 1:1 molar ratio of water to TEOS was used throughout. Zirconium tetrapropoxide was then added with simultaneous addition of water, propanol, and 70 wt% nitric acid to give overall molar ratios of 1 $[M^{4+}]$: 4 H_2O : 4 propanol, 1 mol $[Si^{4+}]$: 15 cm^3 70 wt% HNO_3, and 1 mol $[Zr^{4+}]$: 50 cm^3 70 wt% HNO_3. Gel time was taken as the point when the magnetic stirrer was no longer able to create a vortex while set to 250 rpm. All gels were redispersed in boiling ethyl acetate and refluxed for 4 h, before being transferred to a critical point drying apparatus. The chamber was filled with liquid CO_2 at 298 K before the temperature was raised to 320 K, to give a pressure of 8.685 MPa. The sample then remained in contact with the CO_2 for 4–6 h before the CO_2 was changed while supercritical conditions were maintained. This process was repeated twice daily for 5 days. Calcination was performed at 773 K (2 h) in flowing air. A series of xerogels of identical composition were prepared by omitting the supercritical drying stage.

For comparison purposes, a sample (PPt) was prepared by precipitation of $Zr(OH)_4$ over Aerosil 200 to give a 9 mol% Zr loading (13). The silica was suspended in water containing $Zr(NO_3)_4$ before dropwise addition of 0.365 M ammonia solution. The solid was filtered before being dried at 363 K (16 h) and then calcined in flowing air at 773 K (2 h).

Characterisation

BET surface areas were obtained from single-point ($P/P_0 = 0.3$) measurements at 77 K using Ar as adsorbate. FTIR spectra of the OH stretching region (3800–3400 cm^{-1}) were obtained in the transmittance mode in a quartz cell with CaF_2 windows. Spectra of the samples (80 mg) in the form of 25 mm diameter self-supporting discs were recorded (100 scans at 4 cm^{-1} resolution) following outgassing at 423 and 773 K for 2 h under high vacuum. Discs of 190 mg of KBr and 10 mg of sample were used for investigation of the region below 1250 cm^{-1}.

Acidic properties were determined for samples outgassed *in situ* at 488 K and then exposed to 8 Torr pyridine at 298 K followed by outgassing at 423 K (1 h) and at 488 K (1 h) with spectra recorded at each stage. The mass of pyridine adsorbed under these conditions was obtained by performing identical experiments on a PC-controlled gravimetric balance connected to a conventional vacuum line. The combination of the mass of adsorbed species after desorption at more than one temperature and the integrated absorption values for the appropriate IR bands allowed absorption coefficients, ε in centimeters per micromole, to be determined from which the number of base molecules adsorbed at Lewis and Brønsted sites could be derived.

$$A_i = \frac{\varepsilon_i n_i m}{a_c}$$

where A_i is the integrated absorbance in inverse centimeters due to species i, n_i is the amount of species i adsorbed in micromoles per gram, m is the mass of sample in grams, and a_c is the cross-sectional area in square centimeters of the sample disc. The range of acid site strengths was evaluated by measuring the heats of adsorption of ammonia on samples that were previously outgassed at 423 K and cooled to the adsorption temperature under vacuum. Microcalorimetric measurements were performed using a SETARAM C80 II Tian-Calvet heat flow calorimeter connected to a glass vacuum adsorption chamber. The experimental system is described in detail elsewhere (15). Pulses (ca. 2 μmol) of NH_3 were exposed to 0.045 g of sample at 330 K.

The condensation reaction between acetone and methanol to produce 2,2-dimethoxypropane was used (16) to test the Brønsted acidity of the samples. A 100 cm^3 round-bottom flask fitted with a magnetic stirrer and a water-cooled condenser was immersed in an oil bath maintained at 333 K. Catalyst (60 mg) was introduced to the dry vessel while 5.808 g of acetone (0.1 mol) and 6.408 g of methanol (0.2 mol) were mixed in a separate vessel and added via the condenser. Aliquots of liquid were drawn off at regular intervals and transferred to sealed vials submerged in an ice slurry. The liquid was analysed using a GC fitted with a capillary column and MS detector.

^{29}Si MAS NMR spectra (59.6 MHz) of the samples were obtained using a Chemagnetics CMX300 LITE multinuclear FT spectrometer. Powdered samples contained within 7.5 mm o.d. zirconia "pencil" rotors were spun at 4 kHz using compressed air. Instrument calibration was performed using 3-(trimethylsilyl)-1-propanesulphonic acid sodium salt. ^{29}Si and $^{29}Si\{^1H\}$ CP MAS NMR experiments were performed to determine the proportion of total silanols ($Q^2 + Q^3$) to the total siloxane (Q^4) population and the relative proportions of geminal (Q^2) and single (Q^3) silanols, respectively (17, 18). The relative proportions of the various silicon species were determined by single-pulse and variable contact time (vct) cross-polarisation (CP) measurements. H–Si cross-polarisation times (T_{Si-H}) were obtained by fitting the expression, $M = M_0(1 - \exp(-\tau/T_{Si-H}) \exp(-\tau/T_{1\rho H})$ to plots of M against contact time, τ, of the Q^2, Q^3, and Q^4 components obtained by deconvolution of vct spectra. Longitudinal (spin lattice) relaxation times (T_1) were obtained by using the saturation recovery pulse sequence, $[(\pi/2)_x]_{100} - \tau - (\pi/2)_x$, where τ was varied from 5 to 600 s. T_1 was calculated using the relationship, $M = M_0(1 - \exp(-\tau/T_1)$, where M and M_0 represent intensity at recovery time, τ, and maximum intensity, respectively.

^1H NMR was used to perform cryoporosimetric pore size measurements (19, 20). Powdered samples were mixed with minimal amounts of cyclohexane until just past free flow (theoretically just above pore saturation) and inserted into a rotor and spun at 4 kHz. With the sample at 223 K, proton spectra were acquired as the spin echo amplitude from

a $(\pi/2)$–τ–(π) pulse sequence was measured with a delay time, τ, of 10 ms, to ensure that the signal was entirely from any liquid present (spin–spin relaxation in the solid is typically short, ≈1 ms, for solid cyclohexane, but in excess of 1 s for the liquid). The experiment was repeated numerous times where the integrated signal intensity was measured as a function of temperature and should be proportional to the volume of liquid present. Pore size calculations were made using mathematical techniques applied to the Gibbs–Thomson equation that relates the decrease in melting temperature of a solid to the crystal dimensions (19, 20). A calibration curve for the variation in proton signal intensity with temperature was performed using 2,2-dimethylbutane, which remained liquid across the temperature range used in the cyclohexane proton experiments (mpt 173.25 K, bpt 322.85 K). The intensity variation curve was applied to all data acquired during cryoporosimetric measurements.

RESULTS

Table 1 includes some of the physical characteristics of the samples. The decrease in gelling time with increased zirconia content is expected given that the zirconia precursor is the more reactive alkoxide (21). Under similar conditions, pure zirconia gelled almost instantaneously. Although silica–zirconia samples generally show increased crystallinity with increasing zirconia content (22), samples after calcination at 773 K, even at 75 mol% Zr, were still amorphous to XRD. Consistent with previous observations (6, 21, 23), data in Table 1 show a decrease in BET surface area as the Zr : Si ratio was increased. Xerogels showed consistently lower BET areas than the corresponding aerogel with the higher area samples showing a greater loss (24%) than the lowest area samples (8%).

TABLE 1

Physical Characteristics of the Samples

Sample (mol% Zr)	Gel times (s)	BET ($m^2\ g^{-1}$)[a]	BET ($m^2\ g^{-1}$)[b]
9	1320	351	460
20	256	267	303
33	96	246	283
50	55	204	220
75	19	141	153

[a] Xerogel (produced without supercritical drying in CO_2).
[b] Aerogel.

Figure 1 shows FTIR spectra of the samples after *in situ* outgassing at (A) 423 and (B) 773 K. Low-temperature

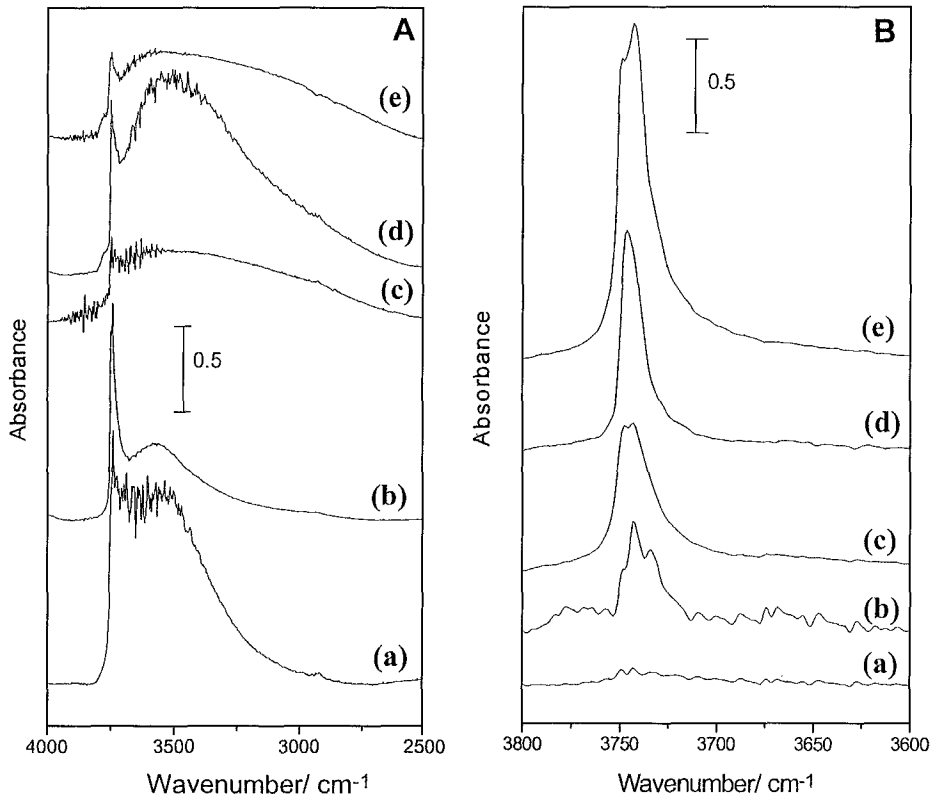

FIG. 1. FTIR spectra in the hydroxyl stretching region after degassing at (A) 423 and (B) 773 K for samples (a) 9, (b) 20, (c) 33, (d) 50 and (e) 75 mol% zirconia.

TABLE 2

Infrared and Gravimetric Data for Pyridine Adsorption

Sample (mol% Zr)	Concentration[a]	A_{1540}[b]	A_{1450}[b]	ε_{1540}[c]	ε_{1450}[c]	$n_{\text{Brønsted}}$[d]	n_{Lewis}[d]
9	103.2 (41.3)	0.800 (0.461)	1.358 (0.481)	1.32	1.49	0.069 (0.028)	0.066 (0.026)
20	268.6 (200.5)	3.113 (2.636)	2.668 (1.565)	1.16	1.58	0.328 (0.278)	0.206 (0.121)
33	207.9 (165.0)	1.316 (0.873)	3.686 (3.139)	1.25	1.58	0.137 (0.091)	0.305 (0.260)
50	169.6 (126.6)	0.968 (0.499)	3.142 (2.621)	1.30	1.56	0.125 (0.064)	0.339 (0.280)
75	214.8 (111.2)	0.667 (0.535)	4.679 (2.169)	1.18	1.59	0.133 (0.107)	0.696 (0.326)

Note. Values obtained after evacuation of pyridine at 423 K (and 488 K).

[a] Micromoles of pyridine per gram sample.

[b] Integrated absorbance (cm^{-1}) of IR band.

[c] IR absorption coefficient (cm μmol^{-1}).

[d] N^0 of acid sites per square nanometer (i.e., N^0 of pyridine molecules retained per square nanometer after evacuation at the specified temperature).

outgassed samples all show a narrow band at ca. 3750 cm^{-1} and a much broader feature with a maximum between 3600 and 3300 cm^{-1}. The former is due to hydroxyls on the silica component of the silica–zirconia aerogels (13) while the latter, which could be removed by increasing the evacuation temperature, is due to adsorbed water. This band, although showing no overall trend, showed a greater degree of tailing to lower frequencies for the higher zirconia-containing samples. These higher Zr/Si ratio samples also contained a shoulder at 3781 cm^{-1} that was not observed at 9 or 20 mol%. This is consistent with previous studies (13) where sol–gel-derived oxides with 9 mol% Zr did not present this feature while samples prepared by precipitation of zirconia did. From published data for the different forms of pure zirconia (24, 25), it was concluded that the latter contained highly dispersed monoclinic phases although the presence of tetragonal and amorphous phases could not be ruled out, while the 9 mol% Zr sol–gel sample did not contain the monoclinic phase. A similar argument here would exclude the presence of monoclinic zirconia for the 9 and 20 mol% samples even though calcination in air at 773 K would be expected to convert any amorphous ZrO_2 present to the monoclinic phase (24). Samples treated at 423 K, show a progressive reduction in intensity of the ca. 3750 cm^{-1} silanol band as the loading increased (except the 33 mol% Zr sample) consistent with the decreasing percentage of silica in the samples. However, from measurement of the relative intensity at ca. 3750 cm^{-1}, the extent to which this decreases is less than expected in relation to the proportion of silica present. After heating of the sample at 773 K, the trend was reversed and the amount of surface silanols remaining was greater for samples with the lowest SiO_2 contents. The surface silanol concentration of the 75 mol% Zr sample was greatest (Fig. 1Be), while the contributions in the other samples was diminished as a function of increasing silica concentration, reaching complete dehydroxylation on the 9 mol% Zr sample (Fig. 1Ba). Expansion of the abscissa scale for the 773 K treated samples reveals splitting of the silanol band. Hydroxyls on zirconia were removed (Fig. 1B) by high-temperature evacuation (24).

IR spectra of adsorbed pyridine revealed bands characteristic of both Lewis (1450 cm^{-1}) and Brønsted (1540 cm^{-1}) forms of adsorption. By combining IR and gravimetric measurements, absorption coefficients could be calculated at each frequency for both forms of adsorbed species (Table 2). These covered a relatively narrow range of values (1.16 to 1.32 at 1540 cm^{-1} for the pyridinium ion and 1.49 to 1.59 at 1450 cm^{-1} for the Lewis bound pyridine) with the average of 1.24 (at 1540 cm^{-1}) and 1.56 (at 1450 cm^{-1}) comparing well with values of 1.23 and 1.57 cm μmol^{-1} for 9 mol% silica zirconias prepared by different methods (13). The absorption coefficients allowed calculation of the surface densities of both types of acid site as detected by pyridine. Figure 2 illustrates the approximately linear increase in Lewis acid site density as the zirconia concentration was increased while the Brønsted acid site density showed a maximum for the sample with 20 mol% and then remained at a constant but non-zero level beyond this concentration. Also shown are values for a sample prepared by precipitation of zirconia over silica microspheres (13). Consistent with the lack of mixing associated with this method and subsequently greater amount of exposed ZrO_2, the sample shows higher Lewis acid density than the sol–gel-derived sample of equivalent Zr content. Despite the lack of mixing, a greater density of Brønsted sites was also produced.

The relationship between acid site density and activity for the acetone and methanol reaction is shown in Table 3. Neither silica nor zirconia samples presented activity for this reaction, confirming that only Brønsted acid sites catalyzed the conversion. Normalization of the values of activity per unit BET surface area allows a comparison between number of protonic sites available and overall activity to be made. General agreement between the relative magnitude of values for the different samples confirms that an

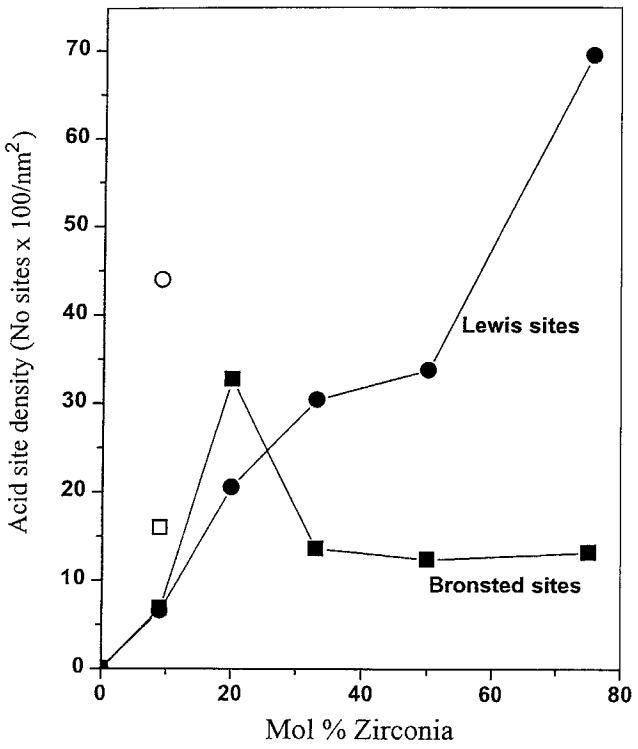

FIG. 2. Plot of Brønsted (squares) and Lewis (circles) acid site densities as a function of mol% zirconia in sol–gel-derived oxides. Open symbols refer to the 9 mol% zirconia sample prepared by precipitation.

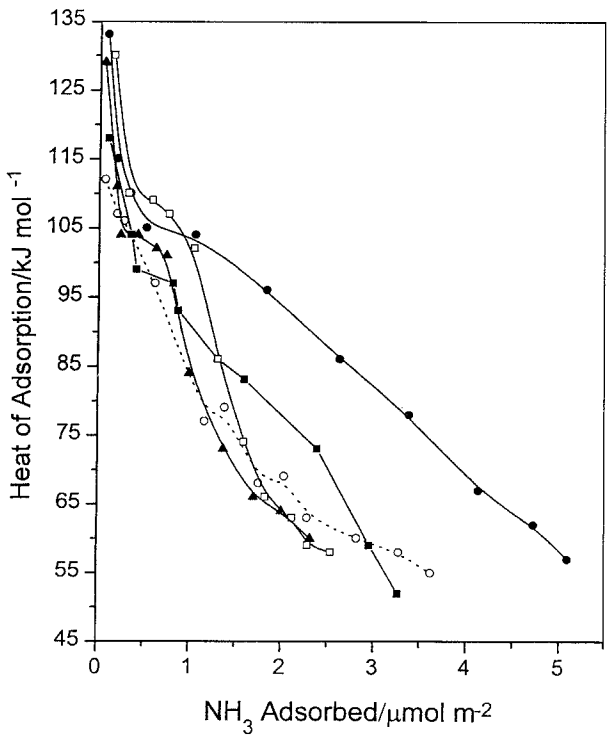

FIG. 3. Plots of heats of adsorption as a function of ammonia coverage for 9 (open squares), 20 (triangle), 33 (open circle), 50 (filled circle), and 75 (filled square) mol% Zr samples outgassed at 423 K.

accurate estimation of Brønsted acid sites has been made. The 20 mol% Zr sample shows the highest activity in line with the greatest density of Brønsted acid sites detected by pyridine while the 9 mol% Zr sample prepared by precipitation shows considerably greater activity that its aerogel counterpart. TOFs calculated on the basis of the number of Brønsted sites detected by pyridine adsorption (Table 3) range between ca. 10–30 for the range of aerogels with the PPt sample exhibiting a greater value. A volcano-shaped plot with maximum at 20 mol% Zr which would be produced by the activity data (Table 3, column 3) would also be produced in a plot of TOF (Table 3, column 4) against mol% Zr, indicating that the acid strength in addition to the densities varied across the series.

TABLE 3

Comparison of Catalytic Activity with Acid Densities Measured by Pyridine Adsorption

Sample (mol% Zr)	Brønsted (and Lewis) site densities (μmol m^{-2} × 10^2)[a]	Activity (mmol min^{-1} m^{-2})[b]	TOF (s^{-1})
9(PPt)	26.6 (73.1)	0.55	34
9	11.5 (11.0)	0.13	19
20	54.5 (34.2)	0.94	29
33	22.8 (50.7)	0.22	16
50	20.8 (56.3)	0.16	13
75	22.2 (115.5)	0.12	9

[a] Calculated from pyridine retained after evacuation at 423 K (values for Lewis acid site densities appear in parentheses).
[b] Calculated from initial conversion of acetone.

Figure 3 shows the heats of adsorption for NH_3 as a function of coverage for samples outgassed at 423 K. Similar profiles suggest some degree of similarity in the nature of the 9 and 20 mol% samples. Samples of 9, 20, and 50 mol% Zr show the highest initial heats of adsorption (ca. 130 kJ mol^{-1}) with the values for the 33 and 75 mol% samples some 15 kJ mol^{-1} lower. The PPt sample gave an even lower q_{initial} value of ca. 110 kJ mol^{-1} (13). Zirconia shows widely differing heats of adsorption profiles and initial heats depending on sample preparation with the latter varying from 85–210 kJ mol^{-1} (27). All samples show some form of plateau below 1 μmol m^{-2}, corresponding quantitatively to the stronger adsorption sites where pyridine was held after evacuation at 423 K (Table 3). The initial values up to this plateau are indicative of NH_3 adsorption at strong Lewis sites (28) while points beyond the plateau indicate adsorption at both weaker Lewis and the Brønsted sites. For higher Zr-containing (50 and 75 mol%) samples, this region is expected to be dominated by adsorption at the former, according to the relative proportions of the sites calculated by C_5H_5N adsorption (Table 3). For the 9, 20, and 33 mol% Zr samples, NH_3 adsorption at Brønsted sites is expected

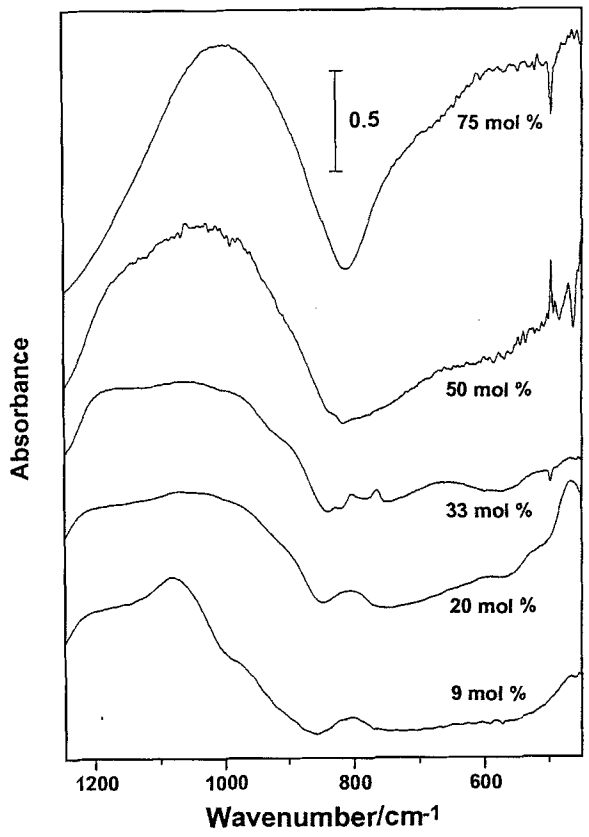

FIG. 4. FTIR spectra of the various mol% zirconia samples in KBr.

to make a more significant contribution to the shape of the adsorption curve beyond the plateau region.

Features corresponding to Si–O–*M* vibrations from analysis of the skeletal vibrational region are often used to provide an indication of the degree of molecular-scale mixing (11). Spectra of samples in KBr show increasing intensities at ca. 3400 and 1630 cm^{-1} as a function of increasing zirconia content (not shown), indicating that hydrophilicity was enhanced by the presence of zirconia. Spectra of silica (Fig. 4) show a broad band between 1250 and 1000 cm^{-1} and two less intense features at 810 and 465 cm^{-1}. The latter pair are due to the symmetric stretching and deformation modes, respectively, while the more intense feature is due to the asymmetric stretching mode. These features are observed in the 9 mol% sample, with specific maxima appearing at 1189, 1081, 986, 807, and 465 cm^{-1} (Fig. 4). As the zirconia content is increased, the spectra become distorted with respect to the pure silica spectrum. The 465 cm^{-1} band is observed clearly only up to 33 mol% Zr. The 807 cm^{-1} band is also lost beyond this Zr concentration and at this loading is split, giving features at 863 and 764 cm^{-1}. The maximum of the most intense feature shifts from 1081 to 1012 cm^{-1} for the 75 mol% Zr sample with the asymmetry to the high wavenumber side eventually being lost. A band at 604 cm^{-1}, not apparent for 9 mol%, appears at 20 mol% and is progressively shifted to 663 and 679 cm^{-1} before appearing as a pronounced shoulder at 715 cm^{-1} for the 75 mol% sample.

^{29}Si MAS NMR experiments gave a broad signal between −75 and −125 ppm, which was deconvoluted to three components with chemical shifts at ca. −90, −100, and −110 ppm attributed (17, 18) to Q^2, Q^3, and Q^4 silicons, respectively. No additional lines with respect to pure silica were required to accurately deconvolute the total signal and so, as for Si–O–Ti units (29), it would appear that the Si–O–Zr bond gives rise to a chemical shift similar to that of Si–O–H. As small values of the cross-polarisation time, T_{Si-H}, indicate protons to be in the spacial vicinity of the Si nuclei, the increase in these values for Q^2 and Q^3 silicons as silica content is decreased (Table 4) is consistent with an increasing proportion of Si–O–Zr linkages relative to Si–O–H and confirms that $(Si–O)_2–(Si)–(O–X)_2$ and $(Si–O)_3–(Si)–(O–X)$ where X = H and/or Zr contribute to Q^2 and Q^3 signals, respectively. The sample 50 mol% appears to be out of step with the general trends for the others in the series. Relative proportions of Q^2, Q^3, and Q^4 silicons from both cross-polarisation and single-pulse experiments are collected in Table 4. Consistent with the expectation that Q^4 signal represents $Si(–O–Si)_4$ units even in the mixed oxides (13, 29), the single-pulse experiments show a progressive decrease in the contribution from Q^4 as the proportion of silica in the samples decreased. This would be expected if the size of the average domain containing only silica decreased with increasing Zr content, as the statistical probability of forming Si–O–Zr linkages increased or

TABLE 4

^{29}Si One-Pulse and CP MAS NMR Contributions

Sample (mol% Zr)	One-pulse Q^4 contribution (%)	CP Q^4 contribution (%)	f_s, $(Q^2+Q^3)/Q^{total}$	f_g, $Q^2/(Q^2+Q^3)$	T_{Si-H} (s)			T_1 (s)
					Q^2	Q^3	Q^4	
9	84.6	58.1	0.15	0.35	0.36	0.30	1.88	32.4
20	71.3	21.3	0.29	0.26	0.45	1.47	2.27	30.8
33	69.1	23.2	0.30	0.26	0.56	0.56	1.53	27.4
50	65.7	37.2	0.34	0.30	0.30	0.32	1.05	26.4
75	25.8	15.3	0.74	0.21	0.78	1.81	10.9	18.0

more SiO_2/ZrO_2 interfaces were created with termination of each domain in SiOH or $Si(OH)_2$ species. The PPt sample gave a Q^4 contribution of 76%, identical to the value for the parent Aerosil 200 silica (13), confirming that no mixing, other than that at the interface between the precipitated layer and the surface of the microspheres, took place.

The Q^4 signals measured by CP make a smaller contribution to the total signal as the distance of effective magnetisation transfer is limited, and has been estimated at between 3.3 and 5.83 Å for a range of silicas (30). The relative size of the silica-only domains can be gauged both from the Q^4 values obtained from ^1H–^{29}Si CP experiments and the relative signal decrease when compared to the one-pulse value if it is assumed that siloxanes dominate in the bulk and silanols predominate at the surface of the domains. The 9 mol% Zr sample shows the smallest percentage decrease in Q^4 from one-pulse to CP measurement; however, the very high (460 $m^2 g^{-1}$) surface area for this sample would place the majority of siloxanes in a region sufficiently close to the surface (and hence close to the proton pool). With the exception of this sample, the others, although showing no specific trend in CP-derived Q^4 values, do show progressively smaller differences between one-pulse and CP measured values as the Zr content was increased.

Values of f_g and f_s (Table 4) do not relate to standard definitions (17) of fraction of geminal silanols and fraction of total silanols, respectively, as Q^2 and Q^3 contain contributions from Si–O–Zr linkages. Values of f_g show no particular trends although the range of values from 0.21 to 0.35 covers the range exhibited by Aerosil 200, the PPt 9 mol% Zr sample, and samples in a previously studied 9 mol% series (13). The f_s values steadily increase with increasing Zr content and then show a huge increase at 75 mol% Zr, indicating that the majority of the silicon atoms present in the sample contain at least one of their oxygen atoms linked to H or Zr rather than to four Si atoms. The spin–lattice relaxation parameter, T_1, has been used to estimate the degree of mixing of silica-containing mixed oxides (14). T_1 values (Table 4) progressively decrease as the fraction of zirconia increases. The value obtained for the PPt sample (117 s) agrees with reported values for Aerosil 200 (13, 14) and for Aerosil 200 with surface coatings of TiO_2 (14).

Figure 5 shows cryoporosimetric curves for samples that exhibited detectable porous structure. The applicability of the technique was verified by carrying out N_2 adsorption–desorption isotherms for the 9 mol% Zr sample which gave a similar pore size distribution plot. Only the 75 mol% Zr gave no indication of pore volume although it is possible that the sample contained micropores below the level of detection of this method due to the use of cyclohexane. Alternatively, the sample may have possessed no internal surface area, consistent with it presenting the lowest (153 $m^2 g^{-1}$) surface area of the series. Only the second highest loaded sample (50 mol% Zr) gave some indication for the presence of micropores while the others gave maxima in distribution profiles in the meso region, with the two lowest loaded samples tailing into the macro region. The overall trend appeared to be a move in the median value to smaller pore diameters with increasing zirconia content. The two lower loaded samples showed a degree of similarity in terms of the overall profiles with the suggestion that three distinct pore types were present for these samples.

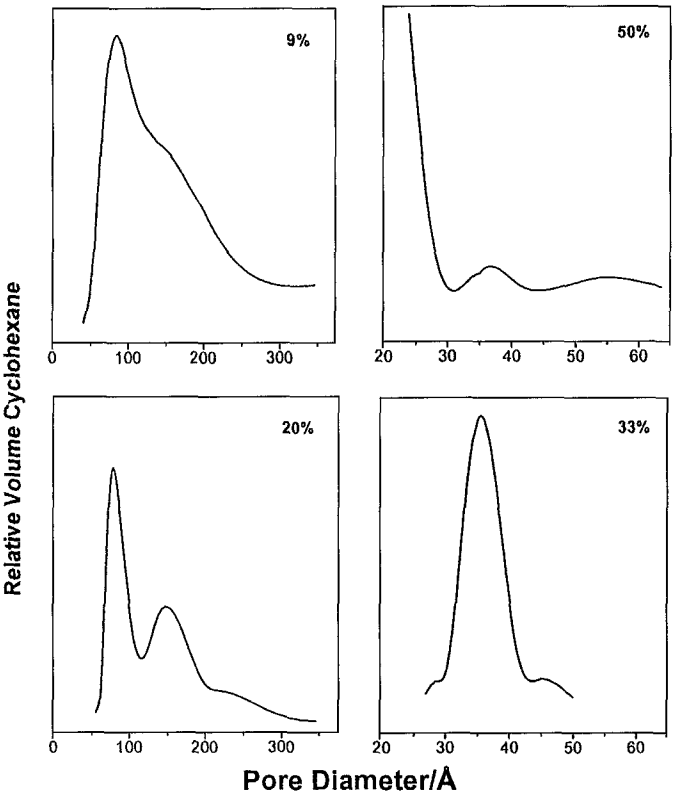

FIG. 5. Pore size distributions from cryoporosimetry using ^1H NMR of cyclohexane.

DISCUSSION

Structure

Samples prepared by the parameters selected here show an exponential decrease in gel time as the Zr : Si ratio was increased consistent with the fact (21, 31) that zirconium alkoxides are more reactive with water than silicon alkoxides. Despite the difficulty in dealing with short gel times and the consequent tendency of high Zr : Si samples to show separation of a crystalline tetragonal zirconia phase when calcined between 673–873 K (21, 32, 33), all samples here using a prehydrolysis approach were X-ray amorphous after calcination at 773 K. Similar high Zr : Si ratio amorphous samples have been reported, but not from alkoxide

precursors (34, 35). Although no XRD evidence was obtained for crystalline phases of zirconia, FTIR spectra of the hydroxyl region (Fig. 1) indicate that small particles of zirconia with monoclinic structure must have been present for samples with mol% Zr > 20, if the band at 3781 cm^{-1} can be used (13) as indicative of hydroxyls specific to this phase (24, 25). This band was also detected for the PPt sample. This is in contrast with a report of zirconia-coated silica where cubic phase ZrO_2 was detected (XRD) but no IR bands due to zirconia hydroxyls (36).

The decrease in BET surface area with increasing Zr : Si ratio is consistent with published observations (5, 6, 21, 34, 35) and with the general finding that Zr-rich gels are more dense than gels with low Zr contents (21). The increased density with mol% Zr is consistent with pore distribution plots (Fig. 5) which show a shift in the median values from 100 to 35 and then into the microporous realm for 50 and possibly 75 mol% Zr samples. Pure zirconia aerogels show volcano-type pore distributions over the 20–1000 Å range with a maximum between 40 and 400 Å which varies according to the acid : alkoxide ratio (37) and supercritical drying temperature (38). The greater volume in smaller pores for the lower Zr : Si samples prepared by Pirard *et al.* (21) contrasts with the findings here and thus extrapolation of pore data for pure zirconia to silica–zirconia to extract information regarding structure may be limited.

Extent of Component Mixing

Miller *et al.* (11, 12, 39) produced a series of high Zr : Si ratio sol–gel samples which showed a range of component distributions but no apparent correlation between mixing and pore size (narrow, intermediate, or broad) distribution (11). However, they claim that a shift in distribution to higher pore size is indicative of well-matched precursor reactivities (12) and therefore increased homogeneity (39). This would suggest that samples here (Fig. 5) show decreasing homogeneity with increasing zirconia content. While this may be used in comparing samples of similar component ratios, its application to a series where the ratio is varied is probably limited, especially in a case such as that of SiO_2–ZrO_2 where Zr-rich gels are more dense than gels of low Zr content (21).

Amongst parameters to determine the "goodness" of mixing, Miller and Ko (11) suggest that the absence of XRD patterns for multicomponent systems is the result of delayed component crystallization which occurs for well-mixed samples. On this basis it would appear that the relatively small proportion of silica was well dispersed through the zirconia network for high Zr : Si samples as large domains of zirconia only would almost certainly appear as crystalline tetragonal phases by comparison with results for zirconia-only aerogels which had been calcined at 773 K (35, 36). Further evidence for the high silica dispersion throughout the highest mol% Zr sample comes from the NMR data which shows a low one-pulse measured Q^4 value (and high f_s) (Table 4), indicative of few Si–$(O–Si)_4$ units but which shows a reasonable drop when measured by cross-polarisation, indicating that the Q^4 units are far from the proton pool and thus most likely located internally, rather than being part of small, silica-rich patches at the surface. This is confirmed by the large Q^4 proton–silicon cross-polarisation time for the 75 mol% Zr sample (Table 4).

The detection of IR bands due to heteroatom linkages is often used (11) to determine the degree of mixing. Spectra (Fig. 4) show trends similar to those of SiO_2–ZrO_2 (5, 37) and other SiO_2-containing oxides (41, 42) with increasing heteroatom concentration. The ν_{asym} Si–O–Si shifts from ca. 1080 cm^{-1} to lower wavenumbers while the 1190 cm^{-1} shoulder becomes part of the main band. The ca. 810 cm^{-1} band due to ν_{sym} Si–O–Si disappears and the 986 cm^{-1} band shifts to lower frequencies and then disappears. The latter band, which appears at ca. 970 cm^{-1} due to ν Si–OH for pure silica (5, 13), increases in intensity for higher temperature treatments of SiO_2–ZrO_2 mixed oxides and with increasing Zr : Si ratios (40), indicating that the band shifting from 986 at low mol% Zr is due to Si–O–Zr linkages (40) rather than modification to an O–H bond (41). The band at 604 cm^{-1}, which appears in Raman spectra of defect silicas due to the presence of three-membered Si–O rings (18), also appears in IR and Raman spectra of zirconia-rich ZrO_2–SiO_2 glasses and zircon (40). The increase in intensity with increasing mol% Zr and progressive shift to higher frequencies make an assignment to vibrations of ZrO_x units (where $x = 7$ or 8) plausable. While comparison of samples of the similar composition may provide information concerning the degree of mixing (11), dramatic changes in the spectra of the varying compositions (Fig. 4), due to contributions from silica-only, zirconia-only, and Si–O–Zr mixed units, make this approach inapplicable in the present study. While Q^2 and Q^3 make increased contributions to total signals as the Zr content is increased (column f_s, Table 4), the decreasing number of silanols in the IR spectra of the 423 K treated samples (Fig. 1A) and general increase in T_{Si-H} values with increasing Zr (Table 4) strongly suggest that Si–O–Zr linkages are formed in the mixed oxides.

One approach, not offered by Miller and Ko (11), to estimate the degree of mixing of multicomponent oxides which has been shown to be useful for Si-containing oxides (14) is the use of spin–lattice relaxation times. Pure silicas show long relaxation times beyond 100 s (13, 14) as do two-component oxides where mixing is limited, such as the PPt sample. The linear decrease in T_1 as a function of decreasing silica concentration (Table 4) suggests progressively smaller domains of silica rather than fewer domains of a similar size which would be an alternative manner in which the decreasing amounts of silica could be dispersed. In the saturation recovery experiments, the rate of the slowest relaxing Si atoms is being presented and this will mainly

involve the siloxanes which are held in the bulk rather than at the surface and in the vicinity of the proton pool. This means that surface area (Table 1) and hydrophobicity (see text for Fig. 4) of the mixed oxide are of secondary importance and the T_1 value truly reflects the dispersion of silicons in the bulk of the oxide and hence the degree of mixing. The linear relationship between T_1 values and zirconia concentration indicates the extent of mixing and homogeneity to be uniform across the series.

Generation of Acid Sites

In line with Tanabe's postulations (2, 4), and results for varying mol ratio silica–zirconias (5, 33) there is a marked increase in Lewis acid density as [Zr] was increased (Fig. 2). While pure silica shows no Lewis acidity, pure zirconias do (4, 5, 24) and so a roughly (Fig. 2) linear increase in Lewis acid site density as a function of mol% Zr may be expected if surface enrichment by silica (35) is avoided. Comparison with the Lewis density for the PPt sample (Fig. 2) where the majority of the zirconia would be available for adsorption indicates that the sol–gel-derived oxides do not present external surfaces where only zirconia is present. While the PPt sample gave one of the highest Lewis acid site densities (Fig. 2) due to a high surface concentration of exposed Zr^{4+} ions, the initial heat of adsorption at 110 kJ mol^{-1} (13) usually thought to reflect adsorption at the strongest Lewis acid sites (26), indicated the sites to be relatively weak. The fact that the 75 mol% Zr sample also gave a high density of Lewis sites (Fig. 2) but a lower than average (117 kJ mol^{-1}) initial heat of adsorption (Fig. 3) compared to the other mixed oxides suggests that whereas samples with large patches of zirconia produce a greater number (or density) of Lewis acid sites, Lewis acid strength was enhanced by a degree of surface mixing between the two components. This is consistent with XPS results (35) where the Zr $3d_{5/2}$ binding energy and thus positive charge on surface Zr cations was greater for mixed oxides than single oxide ZrO_2 and where separation of the two oxides occurred (e.g., at high Zr loadings). Samples with high Zr loadings (50 and 75 mol% Zr) or surfaces enriched in Zr (PPt) and high densities of Lewis sites (Table 3) showed profiles where the large quantity of NH_3 adsorbed with intermediate heats of adsorption compared with lower loaded samples reflects adsorption on silica-free patches of zirconia.

The high incidence of Lewis sites on the 75 mol% Zr sample makes a major contribution to the total (Lewis + Brønsted) density being the highest of the series. This is consistent with data for SiO_2–TiO_2 (42, 43) but contrasts with the maximum at 50 mol% for SiO_2–ZrO_2 (5, 11). However, these authors report total densities of ca. 1 order of magnitude above those obtained here (Table 3), and elsewhere (11) for similar systems, and for other mixed oxides (43). When the same authors report activities for 1-butene isomerisation (6), the number, N, of active sites (in micromoles per square meter) is given as 0.3, 0.47, and 0.13 for the 33, 50, and 67 mol% Zr samples, respectively, which fall in line with the levels of Brønsted acid site densities here. As for 1-butene isomerisation (5, 6, 11), reaction between alcohol and carbonyl to generate the acetal (16) exclusively tests Brønsted acidity. The maximum activity corresponding to the sample (20 mol% Zr) with the greatest number of Brønsted acid sites confirms this assumption (Table 3). Additionally, correlation between the density of sites (second column) and activity (third column) as reflected in a narrow range of TOFs for the aerogels (fourth column) suggests that not only are all sites apparently active, but those detected by pyridine are also available to the reactant molecules (despite differences in pore sizes). Miller and Ko (5) also found that the maximum in reaction rate (isomerisation of 1-butene) for a series of Si/Zr oxides corresponded with the sample with the highest density of Brønsted acid sites, although they found that this sample contained 50 rather than 20 mol% Zr as found here. The Thomas and Tanabe models (3, 4) predict maximum acidity where each oxygen is shared between one Zr and one Si, which given complete mixing of the components would occur at Zr : Si = 0.5 or 33 mol% Zr. Maximum Brønsted acidity at such low Zr : Si ratios contrasts with TiO_2–SiO_2, where high Brønsted acidity is generally found at low mol% silica (43, 44).

While formation of Brønsted acidity and detection of a maximum density for Zr : Si ratios <1 are consistent with the Tanabe model (2, 4), detection of proton acidity for Zr : Si mole ratios >1 contradicts his predictions. Results show (Fig. 2, Table 2) that there is no change in Brønsted acid density on moving from a zirconia minor to major component oxide with similar values for the 33 and 75 mol% Zr samples. The charge imbalance model (2, 4) does not adequately account for the formation of Brønsted acidity at such high Zr : Si ratios. The view that a higher degree of mixing of the components throughout the bulk should be reflected in a greater density of surface Brønsted acid sites (11) is far too simplistic. Comparing the 9 mol% Zr samples, shows that a higher density of Brønsted acid sites is generated (Fig. 2) when internal mixing is restricted by depositing the zirconia over the silica surface by precipitation. The T_1 value for the 9 mol% Zr aerogel (Table 4) reflects (14) a good degree of distribution of the silica component while T_1 for PPt indicates no mixing with respect to the parent silica. It appears that distribution and arrangement of components at the surface rather than in the bulk (11) should be considered when identifying sites for the generation of Brønsted acidity.

It is believed that Brønsted acid sites in SiO_2–ZrO_2 (35, 45, 46) and SiO_2–TiO_2 (22, 39, 42) amorphous mixed oxides are surface silanols, while in zeolites, the site is a hydroxyl at an oxygen atom which bridges the Al and Si atoms (1, 4). Similarity between acidic hydroxyls of zeolites

and those of amorphous silica–aluminas has been proposed (47). Changes in electron density on Si, due to charge imbalance (2, 4, 5, 23) or differences in electronegativity (9, 35, 46), resulting from introduction of a Zr (35, 46) or other (23, 41, 44) atom into the vicinity of the hydroxyl carrying silicon, weakens the SiO–H bond and generates Brønsted acidic sites. The band at 3781 cm^{-1} due to Zr hydroxyls (Fig. 1) is unperturbed with respect to a similar feature on ZrO_2 alone (24, 25) whose single oxide does not, in general, exhibit Brønsted acidity (25, 38). The nonacidic character of the OH is consistent with its high vibrational frequency (high O–H bond strength) and contrasts with low frequencies of ca. 3650 cm^{-1} for acidic hydroxyls on zeolites (1) and silica aluminas (47). Additionally, this band is only prevalent at high Zr : Si ratios (Fig. 1) while high Brønsted acid densities are generated (Fig. 2) at low Zr : Si ratios. It is unlikely that these species participate in the acid-catalysed reaction. Weakening of the SiO–H bond (41) should be reflected in νSiO–H, or the relative ease of thermal desorption.

Prior to evacuation, the 75 mol% Zr sample shows the most adsorbed water, consistent with it showing the highest total acid density (Lewis + Brønsted) and thus the most hydrophilic surface. Calcination at 773 K should render hydrophobic any regions of the surface containing silica only (48), which might be expected for the lowest mol% Zr samples. Evacuation at 423 K revealed that the sample with the highest silica content exhibited the most intense band at 3748 cm^{-1} due to isolated silanols while the amount of water removed by the treatment (broad band at ca. 3500 cm^{-1}) showed no apparent correlation with Zr/Si contents (Fig. 1A). After evacuation at 773 K, the relative intensity of residual OH bands was inverted with respect to the lower temperature treatment, with the hydroxyls of the lowest Zr-containing sample almost completely removed. It is thought that these bands still reflect silicon hydroxyls as the band positions do not exhibit any correlation with hydroxyl species of amorphous or monoclinic zirconias (24, 25). Although no shift in νSiO–H was apparent, with three components at 3748, 3743, and 3733 cm^{-1} observed for each sample (Fig. 1B), the relative ease of dehydroxylation was greatest for the low mol% Zr samples. While it could be argued that the ability to dehydroxylate the surface via condensation was favoured for high Si : Zr ratio samples where larger silica-only patches might exist, thus giving a greater number of neighboring silanols, pure silicas require temperatures of ca. 1400 K for complete dehydroxylation (48). The presence of small amounts of zirconia clearly affected the strength of Si–OH and SiO–H bonds although this influence was diminished as the zirconia content was increased. The 9 mol% Zr sample prepared by precipitation was not highly dehydroxylated by evacuation at 773 K (13) but exhibited greater Brønsted acid density than the corresponding aerogel (Fig. 3). Thus, no correlation between the ease of dehydroxylation (Fig. 1B) and acid site density (Fig. 2) was apparent, although changes in SiO–H bond strength might be expected to influence acid strength rather than number of sites. Unfortunately, intermediate heats of NH_3 adsorption (Fig. 3) reflect both Brønsted and weaker (than initial) Lewis acid sites (26) and no comparisons can be drawn from the calorimetric data and the silanol bond strengths. Zirconia clearly influences silanol bond strengths and some of these may well give rise to Brønsted acidity; however, the actual density of sites created will depend on the distribution and arrangement of components at the surface, rather (5) than throughout the bulk. It is likely that only a very small proportion of the total silanol population (45, 47) exhibits Brønsted acidity.

CONCLUSIONS

Prehydrolysis of silica precursor was effective in matching reactivity with the zirconia alkoxide and avoiding the formation of mixed oxides with silica-enriched surfaces. Effective mixing prevented crystallization of zirconia phases after calcination at 773 K, even at high Zr contents. Sample densities increased as [Zr] was increased with samples going from macroporous (high [Si]) to microporous (high [Zr]). Intermediate ratios of Si : Zr gave rise to narrow-range mesoporous solids. Linear decreases in ^{29}Si T_1 relaxation times and linear increases in Lewis acid site densities as a function of increasing zirconia contents indicated the extent of component mixing to be uniform across the series. Changes in the Si : Zr ratios modified the strength and density of acid groups generated on the mixed oxide surfaces. The highest density of Brønsted acid sites occurred on the 20 mol% Zr samples, while the highest total acid site density occurred at 75 mol% Zr due to the high Lewis site density. Generation of acid sites was not a good indicator of the degree of mixing of the components in the bulk and the exact distribution at the surface is likely to be more significant.

ACKNOWLEDGMENTS

We thank the Carnegie Trust for the Universities of Scotland for a University Studentship and a Travel Grant (C.A.F.) and the Royal Society (London) for a University Research Fellowship (J.A.A.).

REFERENCES

1. Corma, A., *Chem. Rev.* **95**, 559 (1995).
2. Tanabe, K., Sumiyoshi, T., Shibata, K., Kiyoura, T., and Kitagawa, J., *Bull. Chem. Soc. Jpn.* **47**, 1064 (1974).
3. Thomas, C. L., *Ind. Eng. Chem.* **41**, 2564 (1949).
4. Tanabe, K., *in* "Catalysis—Science and Technology" (M. Boudart and J. R. Anderson, Eds), p. 231. Springer-Verlag, Berlin, 1983.
5. Miller, J. B., and Ko, E. I., *J. Catal.* **159**, 58 (1996).
6. Contescu, C., Popa, V. T., Miller, J. B., Ko, E. I., and Schwarz, J. A., *Chem. Eng. J.* **64**, 265 (1996).
7. Kataoka, T., and Dumesic, J. A., *J. Catal.* **112**, 66 (1988).

8. Liu, Z., Tabora, J., and Davis., R., *J. Catal.* **149**, 117 (1994).
9. Kung, H. H., *J. Solid State Chem.* **52**, 191 (1984).
10. Schneider, M., and. Baiker, A., *Catal. Rev.-Sci. Eng.* **37**, 515 (1995).
11. Miller, J. B., and Ko, E. I., *Catal. Today* **35**, 269 (1997).
12. Miller, J. B., Rankin, S. E., and Ko, E. I., *J. Catal.* **148**, 673 (1994).
13. Anderson, J. A., and Fergusson, C. A., *J. Non-Cryst. Solids* **246**, 177 (1999).
14. Anderson, J. A., and Fergusson, C. A., *J. Mater. Sci. Lett.* **18**, 1075 (1999).
15. Bacchiller-Baeza, B., Rodríguez-Ramos, I., and Guerrero-Ruiz, A., *Langmuir* **14**, 3556 (1998).
16. Clark, J. H., *in* "Catalysis of organic reactions by supported Inorganic reagents" (J. H. Clark, Ed.), p. 63, VCH, New York, 1994.
17. Maciel, G. E., and Sindorf, D. W., *J. Am. Chem. Soc.* **102**, 7606 (1980).
18. Humbert, B., *J. Non-Cryst. Solids* **191**, 29 (1995).
19. Jackson, C. L., and McKenna, G. B., *J. Phys. Chem.* **93**, 1990 (1993).
20. Strange, J. H., and Rahman, M., *Phys. Res. Lett.* **71**, 3589 (1993).
21. Pirard, R., Bonhomme, D., Kolibos, S., Pirard, J. P., and Lecloux, A., *J. Sol-Gel Sci. Technol.* **8**, 831 (1997).
22. Meijers, A. C. Q. M., de Jong, A. M., van Gruijthuijsen, L. M. P., and Niemantsverdriet, J. W., *Appl. Catal.* **70**, 53 (1991).
23. Contescu, C., Popa, V. T., Miller, J. B., Ko, E. I., and Schwarz, J. A., *J. Catal.* **157**, 244 (1995).
24. Tret'yakov, N. E., Pozdnyakov, D. V., Orkanskaya, O. M., and Filimanov, V. N., *Russ. J. Phys. Chem.* **44**, 596 (1970).
25. Hertl, W., *Langmuir* **5**, 96 (1989).
26. Cardona-Martinez, N., and Dumesic, J. A., *Adv. Catal.* **38**, 149 (1997).
27. Auroux, A., Artizzu, P., Ferino, I., Solinas, V., Leofanti, G., Padovan, M., Messina, G., and Mansani, R., *J. Chem. Soc. Faraday Trans.* **91**, 3263 (1995).
28. Auroux, A., and Gervasini, A., *J. Phys. Chem.* **94**, 6371 (1990).
29. Walther, K. L., Wokaun, A., Handy, B. E., and Baiker, A., *J. Non-Cryst. Solids* **134**, 47 (1991).
30. Tuel, A., Hommel, H., Legrand, A. P., Chevallier, Y., and Morawski, J. C., *Colloids Surf.* **45**, 413 (1990).
31. Nogami, M., and Nagasaki, K., *J. Non-Cryst. Solids* **109**, 79 (1989)
32. Palladino, M., Pirini, F., Beghi, M., Chiurlo, P., Cogliati, G., and Costa, L., *J. Non-Cryst. Solids* **147**, 335 (1992).
33. Miranda-Salvado, I. M., Serna, C. J., and Fernandez-Navarro, J. M., *J. Non-Cryst. Solids.* **100**, 330 (1988).
34. Navío, J. A., Marchena, F. J., Marcías, M., Colón, G., Avilés, M. A., and Sánchez-Soto, P. J., *J. Sol-Gel Sci. Technol.* **10**, 165 (1997).
35. Bosman, H. J. M., Pijpers, A. P., and Jaspers, A. W. M. A., *J. Catal.* **161**, 551 (1996).
36. Márquez-Alvarez, C., Fierro, J. L. G., Guerrero-Ruiz, A., and Rodríguez-Ramos, I., *J. Colloid Interface Sci.* **159**, 454 (1993).
37. Stöcker, C., and Baiker, A., *J. Non-Cryst. Solids* **223**, 165 (1998).
38. Brodsky, C. J., and Ko, E. I., *J. Non-Cryst. Solids* **186**, 88 (1995).
39. Miller, J. B., and Ko, E. I., *J. Catal.* **153**, 194 (1995).
40. Lee, S. W., and Condrate, R. A., Sr., *J. Mater. Sci.* **23**, 2951 (1988).
41. Sohn, J. R., and Jang, H. J., *J. Catal.* **132**, 563 (1991).
42. Sheng, T.-C., Lang, S., Morrow, B. A., and Gay, I. D., *J. Catal.* **148**, 341 (1994).
43. Doolin, P. K., Alerasool, S., Zalewski, D. J., and Hoffman, J. F., *Catal. Lett.* **25**, 209 (1994).
44. Miller, J. B., Johnston, S. T., and Ko, E. I., *J. Catal.* **150**, 311 (1994).
45. Niwa, M., Katada, N., and Murakami, Y., *J. Catal.* **134**, 340 (1992).
46. Yamaguchi, T., Morita, T., Salama, T. M., and Tanabe, K., *Catal. Lett.* **4**, 1 (1996).
47. Borovkov, V. Y., Alexeev, A. A., and Kazansky, V. B., *J. Catal.* **80**, 462 (1983).
48. Morrow, B. A., *Stud. Surf. Sci. Catal. A* **57**, 160 (1994).